Health and Labor Sciences Research Grants for Comprehensive Research on Disability Health and Welfare (H23-seishin-ippan-002 to RT); Intramural Research Grant for Neurological and Psychiatric Disorders of NCNP (No. 23-10 to RT); and by the Japan Research Foundation for Clinical Pharmacology (to RT). The sponsors had no role in the study design, data collection, data analysis, data interpretation, or writing of the report. The corresponding author had full access to all data in this study, and had the final responsibility in the decision to submit this work for publication.

Contributors

Masato Fukuda, Ryu Takizawa, and Kiyoto Kasai designed the study and wrote the protocol. Ryu Takizawa, Kohei Marumo, and Shingo Kawasaki undertook the statistical analysis. Marumo Kohei, Ryu Takizawa, Masaru Kinou, Yuki Kawakibo, and Kiyoto Kasai conducted data acquisition. Ryu Takizawa and Marumo Kohei wrote the first draft of the manuscript, and the other authors revised it critically for important intellectual content. All authors have approved the final version of the manuscript.

Acknowledgments

The authors gratefully thank all the participants in this study. This study is based on part of a PhD thesis by Dr. Marumo submitted to the University of Tokyo.

Conflict of interest

Regarding financial and material support for the present study, Dr. Kasai has a potential conflict of interest (see below for details). All other authors have no relevant conflict of interest.

Beginning July 31, 2003 and continuing to the present, the University of Tokyo and the Hitachi Group (Advanced Research Laboratory, Hitachi Ltd. and The Research and Developmental Center, Hitachi Medical Corporation) have had an official contract for a collaborative study on the clinical applications of near-infrared spectroscopy (NIRS) in psychiatric disorders, which has been approved by the Research Promotion Office, University of Tokyo Hospital. The principal investigator of this study is Kiyoto Kasai. For this study, Hitachi Medical Corporation provided a project grant (JPY 300,000 per year) and material support (temporary rental of a near-infrared spectroscopy machine (Optical Topography) machine, ETG-4000).

Appendix A. Supplementary data

Supplementary data to this article can be found online at http://dx.doi.org/10.1016/j.neuroimage.2013.04.050.

References

Aloia, M.S., Gourovitch, M.L., Missar, D., Pickar, D., Weinberger, D.R., Goldberg, T.E., 1998. Cognitive substrates of thought disorder, II: specifying a candidate cognitive mechanism. Am. J. Psychiatry 155, 1677–1684.

Alvarez, J.A., Emory, E., 2006. Executive function and the frontal lobes: a meta-analytic review. Neuropsychol. Rev. 16, 17–42.

American Psychiatric Association, 1994. Diagnostic and Statistical Manual of Mental Disorders, 4th ed. American Psychiatric Publishing Inc., Washington, DC.

Assaf, M., Rivkin, P.R., Kuzu, C.H., Calhoun, V.D., Kraut, M.A., Groth, K.M., Yassa, M.A., Hart Jr., J., Pearlson, G.D., 2006. Abnormal object recall and anterior cingulate overactivation correlate with formal thought disorder in schizophrenia. Biol. Psychiatry 59, 452–459.

Barrera, A., McKenna, P.J., Berrios, G.E., 2005. Formal thought disorder in schizophrenia: an executive or a semantic deficit? Psychol. Med. 35, 121–132.

Bleuler, E., 1911/1956. Dementia Praecox or the Group of Schizophrenias. International Universities Press, New York.

Bokat, C.E., Goldberg, T.E., 2003. Letter and category fluency in schizophrenic patients: a meta-analysis. Schizophr. Res. 64, 73–78.

Cabeza, R., Nyberg, L., 2000. Imaging cognition II: an empirical review of 275 PET and fMRI studies. J. Cogn. Neurosci. 12, 1–47.

Cohen, J., 1988. Statistical Power Analysis for the Behavioral Sciences, 2nd ed. Erlbaum, Hillsdale, NJ.

Costafreda, S.G., Fu, C.H., Lee, L., Everitt, B., Brammer, M.J., David, A.S., 2006. A systematic review and quantitative appraisal of fMRI studies of verbal fluency: role of the left inferior frontal gyrus. Hum. Brain Mapp. 27, 799–810.

DeFreitas, C.M., Dunaway, L.A., Torres, I.J., 2009. Preferential semantic fluency impairment is related to hallucinations, but not formal thought disorder. Schizophr. Res. 107, 307–312.

Docherty, A.R., Berenbaum, H., Kerns, J.G., 2011. Alogia and formal thought disorder: differential patterns of verbal fluency task performance. J. Psychiatr. Res. 45, 1352–1357.

Doughty, O.J., Done, D.J., 2009. Is semantic memory impaired in schizophrenia? A systematic review and meta-analysis of 91 studies. Cogn. Neuropsychiatry 14, 473–509.

Ehlis, A.C., Herrmann, M.J., Plichta, M.M., Fallgatter, A.J., 2007. Cortical activation during two verbal fluency tasks in schizophrenic patients and healthy controls as assessed by multi-channel near-infrared spectroscopy. Psychiatry Res. 156, 1–13.

Elvevag, B., Weinstock, D.M., Akil, M., Kleinman, J.E., Goldberg, T.E., 2001. A comparison of verbal fluency tasks in schizophrenic patients and normal controls. Schizophr. Res. 51, 119–126.

Frith, C.D., Friston, K.J., Herold, S., Silbersweig, D., Fletcher, P., Cahill, C., Dolan, R.J., Frackowiak, R.S., Liddle, P.F., 1995. Regional brain activity in chronic schizophrenic patients during the performance of a verbal fluency task. Br. J. Psychiatry 167, 343–349.

Goldberg, T.E., Aloia, M.S., Gourovitch, M.L., Missar, D., Pickar, D., Weinberger, D.R., 1998. Cognitive substrates of thought disorder, I: the semantic system. Am. J. Psychiatry 155, 1671–1676.

Henry, J.D., Crawford, J.R., 2005. A meta-analytic review of verbal fluency deficits in schizophrenia relative to other neurocognitive deficits. Cogn. Neuropsychiatry 10, 1–33.

Hollingshead, A.B., 1965. Two-factor Index of Social Position. Yale University Press, New Haven, U.S.A.

Hoshi, Y., Kobayashi, N., Tamura, M., 2001. Interpretation of near-infrared spectroscopy signals: a study with a newly developed perfused rat brain model. J. Appl. Physiol. 90, 1657–1662.

Hurford, I.M., Marder, S.R., Keefe, R.S., Reise, S.P., Bilder, R.M., 2011. A brief cognitive assessment tool for schizophrenia: construction of a tool for clinicians. Schizophr. Bull. 37, 538–545.

Ikezawa, K., Iwase, M., Ishii, R., Azechi, M., Canuet, L., Ohi, K., Yasuda, Y., Iike, N., Kurimoto, R., Takahashi, H., Nakahachi, T., Sekiyama, R., Yoshida, T., Kazui, H., Hashimoto, R., Takeda, M., 2009. Impaired regional hemodynamic response in schizophrenia during multiple prefrontal activation tasks: a two-channel near-infrared spectroscopy study. Schizophr. Res. 108, 93–103.

Kay, S.R., Fiszbein, A., Opler, L.A., 1987. The positive and negative syndrome scale (PANSS) for schizophrenia. Schizophr. Bull. 13, 261–276.

Kameyama, M., Fukuda, M., Yamagishi, Y., Sato, T., Uehara, T., Ito, M., Suto, T., Mikuni, M., 2006. Frontal lobe function in bipolar disorder: a multichannel near-infrared spectroscopy study. Neuroimage 29, 172–184.

Kaplan, R.D., Szechtman, H., Franco, S., Szechtman, B., Nahmias, C., Garnett, E.S., List, S., Cleghorn, J.M., 1993. Three clinical syndromes of schizophrenia in untreated subjects: relation to brain glucose activity measured by positron emission tomography (PET). Schizophr. Res. 11, 47–54.

Kerns, J.G., Berenbaum, H., 2002. Cognitive impairments associated with formal thought disorder in people with schizophrenia. J. Abnorm. Psychol. 111, 211–224.

Kircher, T.T., Liddle, P.F., Brammer, M.J., Williams, S.C., Murray, R.M., McGuire, P.K., 2001. Neural correlates of formal thought disorder in schizophrenia: preliminary findings from a functional magnetic resonance imaging study. Arch. Gen. Psychiatry 58, 769–774.

Kremen, W.S., Seidman, L.J., Faraone, S.V., Tsuang, M.T., 2003. Is there disproportionate impairment in semantic or phonemic fluency in schizophrenia? J. Int. Neuropsychol. Soc. 9, 79–88.

Kubota, Y., Toichi, M., Shimizu, M., Mason, R.A., Coconcea, C.M., Findling, R.L., Yamamoto, K., Calabrese, J.R., 2005. Prefrontal activation during verbal fluency tests in schizophrenia — a near-infrared spectroscopy (NIRS) study. Schizophr. Res. 77, 65–73.

Liddle, P.F., Friston, K.J., Frith, C.D., Hirsch, S.R., Jones, T., Frackowiak, R.S., 1992. Patterns of cerebral blood flow in schizophrenia. Br. J. Psychiatry 160, 179–186.

Magaud, E., Kebir, O., Gut, A., Willard, D., Chauchot, F., Olie, J.P., Kazes, M., Krebs, M.O., 2010. Altered semantic but not phonological verbal fluency in young help-seeking individuals with ultra high risk of psychosis. Schizophr. Res. 123, 53–58.

Marumo, K., Takizawa, R., Kawakubo, Y., Onitsuka, T., Kasai, K., 2009. Gender difference in right lateral prefrontal hemodynamic response while viewing fearful faces: a multi-channel near-infrared spectroscopy study. Neurosci. Res. 63, 89–94.

Matsuoka, K., Uno, M., Kasai, K., Koyama, K., Kim, Y., 2006. Estimation of premorbid IQ in individuals with Alzheimer's disease using Japanese ideographic script (Kanji) compound words: Japanese version of National Adult Reading Test. Psychiatry Clin. Neurosci. 60, 332–339.

McGuire, P.K., Quested, D.J., Spence, S.A., Murray, R.M., Frith, C.D., Liddle, P.F., 1998. Pathophysiology of 'positive' thought disorder in schizophrenia. Br. J. Psychiatry 173, 231–235.

Obrig, H., Villringer, A., 2003. Beyond the visible — imaging the human brain with light. J. Cereb. Blood Flow Metab. 23, 1–18.

Oldfield, R.C., 1971. The assessment and analysis of handedness: the Edinburgh inventory. Neuropsychologia 9, 97–113.

Reif, A., Schecklmann, M., Eirich, E., Jacob, C.P., Jarczok, T.A., Kittel-Schneider, S., Lesch, K.P., Fallgatter, A.J., Ehlis, A.C., 2011. A functional promoter polymorphism of neuronal nitric oxide synthase moderates prefrontal functioning in schizophrenia. Int. J. Neuropsychopharmacol. 14, 887–897.

Ruff, R.M., Light, R.H., Parker, S.B., Levin, H.S., 1997. The psychological construct of word fluency. Brain Lang. 57, 394–405.

Shenton, M.E., Kikinis, R., Jolesz, F.A., Pollak, S.D., LeMay, M., Wible, C.G., Hokama, H., Martin, J., Metcalf, D., Coleman, M., et al., 1992. Abnormalities of the left temporal lobe and thought disorder in schizophrenia. A quantitative magnetic resonance imaging study. N. Engl. J. Med. 327, 604–612.

Snitz, B.E., Macdonald III, A.W., Carter, C.S., 2006. Cognitive deficits in unaffected first-degree relatives of schizophrenia patients: a meta-analytic review of putative endophenotypes. Schizophr. Bull. 32, 179–194.
Spitzer, M., 1997. A cognitive neuroscience view of schizophrenic thought disorder. Schizophr. Bull. 23, 29–50.
Strangman, G., Boas, D.A., Sutton, J.P., 2002. Non-invasive neuroimaging using near-infrared light. Biol. Psychiatry 52, 679–693.
Suga, M., Uetsuki, M., Takizawa, R., Araki, T., Kasai, K., 2011. Phonological fluency is uniquely impaired in Japanese-speaking schizophrenia patients: confirmation study. Psychiatry Clin. Neurosci. 65, 672–675.
Sumiyoshi, C., Sumiyoshi, T., Matsui, M., Nohara, S., Yamashita, I., Kurachi, M., Niwa, S., 2004. Effect of orthography on the verbal fluency performance in schizophrenia: examination using Japanese patients. Schizophr. Res. 69, 15–22.
Suto, T., Fukuda, M., Ito, M., Uehara, T., Mikuni, M., 2004. Multichannel near-infrared spectroscopy in depression and schizophrenia: cognitive brain activation study. Biol. Psychiatry 55, 501–511.
Takizawa, R., Kasai, K., Kawakubo, Y., Marumo, K., Kawasaki, S., Yamasue, H., Fukuda, M., 2008. Reduced frontopolar activation during verbal fluency task in schizophrenia: a multi-channel near-infrared spectroscopy study. Schizophr. Res. 99, 250–262.
Takizawa, R., Hashimoto, K., Tochigi, M., Kawakubo, Y., Marumo, K., Sasaki, T., Fukuda, M., Kasai, K., 2009a. Association between sigma-1 receptor gene polymorphism and prefrontal hemodynamic response induced by cognitive activation in schizophrenia. Prog. Neuropsychopharmacol. Biol. Psychiatry 33, 491–498.
Takizawa, R., Tochigi, M., Kawakubo, Y., Marumo, K., Sasaki, T., Fukuda, M., Kasai, K., 2009b. Association between catechol-O-methyltransferase Val108/158Met genotype and prefrontal hemodynamic response in schizophrenia. PLoS One 4, e5495.
Tsuzuki, D., Jurcak, V., Singh, A.K., Okamoto, M., Watanabe, E., Dan, I., 2007. Virtual spatial registration of stand-alone fNIRS data to MNI space. Neuroimage 34, 1506–1518.
Tzourio-Mazoyer, N., Landeau, B., Papathanassiou, D., Crivello, F., Etard, O., Delcroix, N., Mazoyer, B., Joliot, M., 2002. Automated anatomical labeling of activations in SPM using a macroscopic anatomical parcellation of the MNI MRI single-subject brain. Neuroimage 15, 273–289.
van der Gaag, M., Cuijpers, A., Hoffman, T., Remijsen, M., Hijman, R., de Haan, L., van Meijel, B., van Harten, P.N., Valmaggia, L., de Hert, M., Wiersma, D., 2006a. The five-factor model of the Positive and Negative Syndrome Scale I: confirmatory factor analysis fails to confirm 25 published five-factor solutions. Schizophr. Res. 85, 273–279.
van der Gaag, M., Hoffman, T., Remijsen, M., Hijman, R., de Haan, L., van Meijel, B., van Harten, P.N., Valmaggia, L., de Hert, M., Cuijpers, A., Wiersma, D., 2006b. The five-factor model of the Positive and Negative Syndrome Scale II: a ten-fold cross-validation of a revised model. Schizophr. Res. 85, 280–287.
Verhoeven, K.J.F., Simonsen, K.L., McIntyre, L.M., 2005. Implementing false discovery rate control: increasing your power. Oikos 108, 643–647.
Yurgelun-Todd, D.A., Waternaux, C.M., Cohen, B.M., Gruber, S.A., English, C.D., Renshaw, P.F., 1996. Functional magnetic resonance imaging of schizophrenic patients and comparison subjects during word production. Am. J. Psychiatry 153, 200–205.

NeuroImage 83 (2013) 158–173

Contents lists available at ScienceDirect

NeuroImage

journal homepage: www.elsevier.com/locate/ynimg

A NIRS–fMRI investigation of prefrontal cortex activity during a working memory task

Hiroki Sato [a,*,1], Noriaki Yahata [b,e,1], Tsukasa Funane [a], Ryu Takizawa [b,f], Takusige Katura [a], Hirokazu Atsumori [a], Yukika Nishimura [b,d], Akihide Kinoshita [b], Masashi Kiguchi [a], Hideaki Koizumi [a], Masato Fukuda [c], Kiyoto Kasai [b]

[a] Hitachi, Ltd., Central Research Laboratory, Hatoyama, Saitama 350-0395, Japan
[b] Department of Neuropsychiatry, Graduate School of Medicine, The University of Tokyo, Bunkyo-ku, Tokyo 113-8655, Japan
[c] Department of Psychiatry and Human Behavior, Gunma University Graduate School of Medicine, Maebashi, Gunma 371-8511, Japan
[d] Department of Youth Mental Health, Graduate School of Medicine, The University of Tokyo, Bunkyo-ku, Tokyo 113-8655, Japan
[e] Global Center of Excellence (COE) Program: "Comprehensive Center of Education and Research for Chemical Biology of the Diseases", The University of Tokyo, Bunkyo-ku, Tokyo 113-0033, Japan
[f] MRC Social, Genetic and Developmental Psychiatry Centre, Institute of Psychiatry, King's College London, London, SE5 8AF, UK

ARTICLE INFO

Article history:
Accepted 12 June 2013
Available online 21 June 2013

Keywords:
Functional magnetic resonance imaging (fMRI)
Near-infrared spectroscopy (NIRS)
Optical topography
Blood oxygenation level dependent (BOLD)
Hemoglobin
Prefrontal cortex
Simultaneous measurement
Working memory
Finger tapping

ABSTRACT

Near-infrared spectroscopy (NIRS) is commonly used for studying human brain function. However, several studies have shown that superficial hemodynamic changes such as skin blood flow can affect the prefrontal NIRS hemoglobin (Hb) signals. To examine the criterion-related validity of prefrontal NIRS-Hb signals, we focused on the functional signals during a working memory (WM) task and investigated their similarity with blood-oxygen-level-dependent (BOLD) signals simultaneously measured by functional magnetic resonance imaging (fMRI). We also measured the skin blood flow with a laser Doppler flowmeter (LDF) at the same time to examine the effect of superficial hemodynamic changes on the NIRS-Hb signals. Correlation analysis demonstrated that temporal changes in the prefrontal NIRS-Hb signals in the activation area were significantly correlated with the BOLD signals in the gray matter rather than those in the soft tissue or the LDF signals. While care must be taken when comparing the NIRS-Hb signal with the extracranial BOLD or LDF signals, these results suggest that the NIRS-Hb signal mainly reflects hemodynamic changes in the gray matter. Moreover, the amplitudes of the task-related responses of the NIRS-Hb signals were significantly correlated with the BOLD signals in the gray matter across participants, which means participants with a stronger NIRS-Hb response showed a stronger BOLD response. These results thus provide supportive evidence that NIRS can be used to measure hemodynamic signals originating from prefrontal cortex activation.

Introduction

Human tissue is highly transparent to light in the visible to near-infrared region, so this region is called the "biological optical window." Millikan's development of a spectroscopic method for estimating the oxygen saturation of blood in human tissue (Millikan, 1942) was followed by the development of the near-infrared spectroscopy (NIRS) technique for noninvasive measurement of tissue oxygenation in the brain (Jöbsis, 1977; Jöbsis-VanderVliet et al., 1988). Particularly important has been the application of NIRS to the measurement of hemodynamic signals related to functional activation in the brain (Chance et al., 1993; Hoshi and Tamura, 1993; Kato et al., 1993; Villringer et al., 1993). The NIRS technique measures relative changes in the concentration of oxygenated hemoglobin (Hb) and deoxygenated Hb (oxy-Hb signal and deoxy-Hb signal, respectively), taking advantage of the difference in absorption coefficients between oxy-Hb and deoxy-Hb depending on the light wavelength (Wray et al., 1988).

From a theoretical viewpoint, the origin of the NIRS deoxy-Hb signal is assumed to be the same as that of the blood oxygenation level-dependent (BOLD) signal in functional magnetic resonance imaging (fMRI), which is sensitive to changes in the concentration of deoxy-Hb in local blood vessels (Ogawa et al., 1990a, 1990b). After a NIRS imaging technique (optical topography) with multiple measurement positions was introduced (Maki et al., 1995; Yamashita et al., 1996), a number of studies using NIRS were conducted in various fields as it offers several advantages. For example, its imposition of fewer body constraints facilitates measurement of the infant brain (Homae et al., 2010; Minagawa-Kawai et al., 2011; Pena et al., 2003; Sato et al., 2012; Taga et al., 2003) and of activations during

* Corresponding author. Fax: +81 49 296 6005.
E-mail address: hiroki.sato.ry@hitachi.com (H. Sato).
[1] These authors contributed equally to this work.

1053-8119/$ – see front matter © 2013 Elsevier Inc. All rights reserved.
http://dx.doi.org/10.1016/j.neuroimage.2013.06.043

walking (Atsumori et al., 2010; Miyai et al., 2001) and communication (Cui et al., 2012; Funane et al., 2011), which are more difficult with fMRI. Moreover, NIRS is easier to administer and less expensive than fMRI, meaning that it will open up new applications.

Although NIRS has certain advantages compared to fMRI, it has a limited measurement depth and less spatial resolution. A potential problem currently drawing attention is contamination of the measurement data due to extracranial hemodynamic changes such as skin blood flow (Germon et al., 1994, 1998; Kirilina et al., 2012; Kohno et al., 2007; Takahashi et al., 2011; Toronov et al., 2001). Given the measurement principle of NIRS, it would not be surprising to find that NIRS-Hb signals contain information reflecting superficial hemodynamic changes mainly due to systemic changes. Therefore, researchers have placed special emphasis on their task paradigms and statistical analysis to ensure extraction of pure brain activity. Although this approach is valid if the assumption holds that extracranial hemodynamics is independent of the task sequence or at least negligible in obtaining brain activity, recent studies have suggested that superficial hemodynamic changes such as skin blood flow are a considerable source of the task-related signals, especially in the frontal area (Kirilina et al., 2012; Takahashi et al., 2011). For example, Takahashi et al. (2011) suggested that the majority of NIRS-Hb signal changes in the forehead reflected the skin blood flow during a verbal fluency task (VFT). The main evidence for this conclusion was derived from an experiment showing that the VFT-related signal changes disappeared when the participants manually pressed a portion of the skin in the measurement area (Takahashi et al., 2011). Moreover, Kirilina et al. (2012) showed task-evoked hemodynamic changes in the superficial forehead region during a continuous performance task. They attributed this task-evoked artifact to systemic changes in the veins draining the scalp, as shown by fMRI results in which similar task-evoked extracranial changes were localized in the superficial frontal veins (Kirilina et al., 2012). Given these results, there is concern that significant artifacts from extracranial hemodynamics in the NIRS-Hb signals may be present in a wide range of cognitive studies. However, the impact of the extracranial artifacts, including their significance and generality, has not been clarified, let alone their true origin and mechanism.

Before clarifying the effect of extracranial artifacts in NIRS measurements, the present study used simultaneous NIRS and fMRI measurements to investigate the validity of using NIRS to measure prefrontal activity during a reliable task. The BOLD signal of fMRI has relatively accurate spatial information and is proportional to the hemodynamic changes that can be measured using NIRS (Buxton et al., 2004; Toronov et al., 2003). It is therefore possible to evaluate the criterion-related validity of the NIRS-Hb signal by comparing it with the corresponding BOLD signal. Of the numerous studies using simultaneous NIRS–fMRI measurements, two recent ones have investigated prefrontal cortex (PFC) activation (Cui et al., 2011; Heinzel et al., 2013). Although they showed a wide regional and inter-individual variability in the NIRS–BOLD correlations around the PFC (Cui et al., 2011; Heinzel et al., 2013), they not fully demonstrate the correlation level in the focused-upon activation region.

Given this background, we examined in more detail to what extent the prefrontal NIRS-Hb signals showing task-related changes are correlated with the BOLD signals. To confirm the generality of the results for the PFC, sensorimotor areas were also measured using a finger tapping task (TAP). The sensorimotor activations mainly in the precentral and postcentral gyri have been well examined in a number of simultaneous NIRS–fMRI studies and have been shown to have high correlation with the signals (Huppert et al., 2006; Kleinschmidt et al., 1996; Mehagnoul-Schipper et al., 2002; Sassaroli et al., 2006; Strangman et al., 2002; Toronov et al., 2001). Of particular interest, Mehagnoul-Schipper et al. (2002) showed that the amplitudes of the deoxy-Hb signals corresponding to task-related changes were significantly correlated with those of the BOLD signals in the left motor cortex. This amplitude correlation is important because it indicates that equivalent statistical results are expected in the two modalities. However, this amplitude correlation has been reported only by Mehagnoul-Schipper et al. (2002), and it naturally remains unclear in the case of PFC activation.

Therefore, the first objective of the present study was to demonstrate a similar amplitude correlation between NIRS and BOLD in PFC activation signals. The second objective was to determine the correlation of NIRS-Hb signals not only with the BOLD signals in the gray matter (GM) layer but also with the BOLD signals in the soft tissue (ST) layer and the skin blood flow measured with a laser Doppler flowmeter (LDF). This approach should provide helpful information about the effect of superficial hemodynamic changes on the prefrontal NIRS-Hb signals. Although weaker signal intensities are expected in ST regions compared to GM regions, the usefulness of ST BOLD signals has been suggested (Heinzel et al., 2013; Kirilina et al., 2012).

We used a working memory (WM) task with a classical delayed response paradigm as a reliable cognitive task for measuring PFC activity. A region of the dorsolateral PFC, Brodmann area (BA) 46, has been shown to be involved in this task through a number of animal electrophysiological studies (Goldman-Rakic, 1987; Kubota and Niki, 1971; Tsujimoto and Postle, 2012) and human neuroimaging studies (D'Esposito, 2007; McCarthy et al., 1994, 1996). Several NIRS studies have also demonstrated PFC activation during a WM task both in children (Tsujimoto et al., 2004) and adults (Aoki et al., 2011, 2013; Sato et al., 2011a). By focusing on activity in BA 46 during the WM task, we expected to achieve more reliable signals from the cerebral cortex.

Materials and methods

Participants

Twenty-seven volunteers (23 males and 4 females, mean age of 36.4, age range of 28–48) participated in the simultaneous NIRS and fMRI measurements. All participants were native Japanese speakers and gave written informed consent to the study protocol, which was approved by the ethical committee of the Faculty of Medicine, the University of Tokyo (No. 3156-(2)). None of these participants had a history of psychiatric or neurological illness, serious head injury, or psychotropic drug use.

Experimental setup and task sequence

The participant was fitted with NIRS probe holders (see Section NIRS for more details) and wore a nonmagnetic headphone (Hitachi Advanced Systems Corp., Japan) for auditory presentation. After the participant lay down on a scanner bed, an LDF probe was centered between the eyebrows, and another one was placed over the left temple. A head coil was placed on his or her head, and mirrors were placed on the head coil to enable the participant to see a screen positioned at his or her feet.

Two task sessions were conducted for each participant: a verbal working memory (WM) task and a finger tapping (TAP) task. The functional activation signals during task performance were measured using NIRS and fMRI. A commercially available software package (E-prime, Psychology Software Tools, Inc., U.S.A.) was used to present visual and auditory stimuli, to synchronize the stimuli presentation to the fMRI scanning, to send serial commands to the NIRS system for recording the time of presentation, and to record the participant's responses for the WM task. A TAP task session was conducted after the WM task session for all participants. A verbal fluency task session was also conducted for another purpose, and the results for that session will be reported elsewhere.

Verbal working memory task

A conventional delayed-response paradigm was used as the verbal WM task (Fig. 1A). It was basically the same as that used in previous

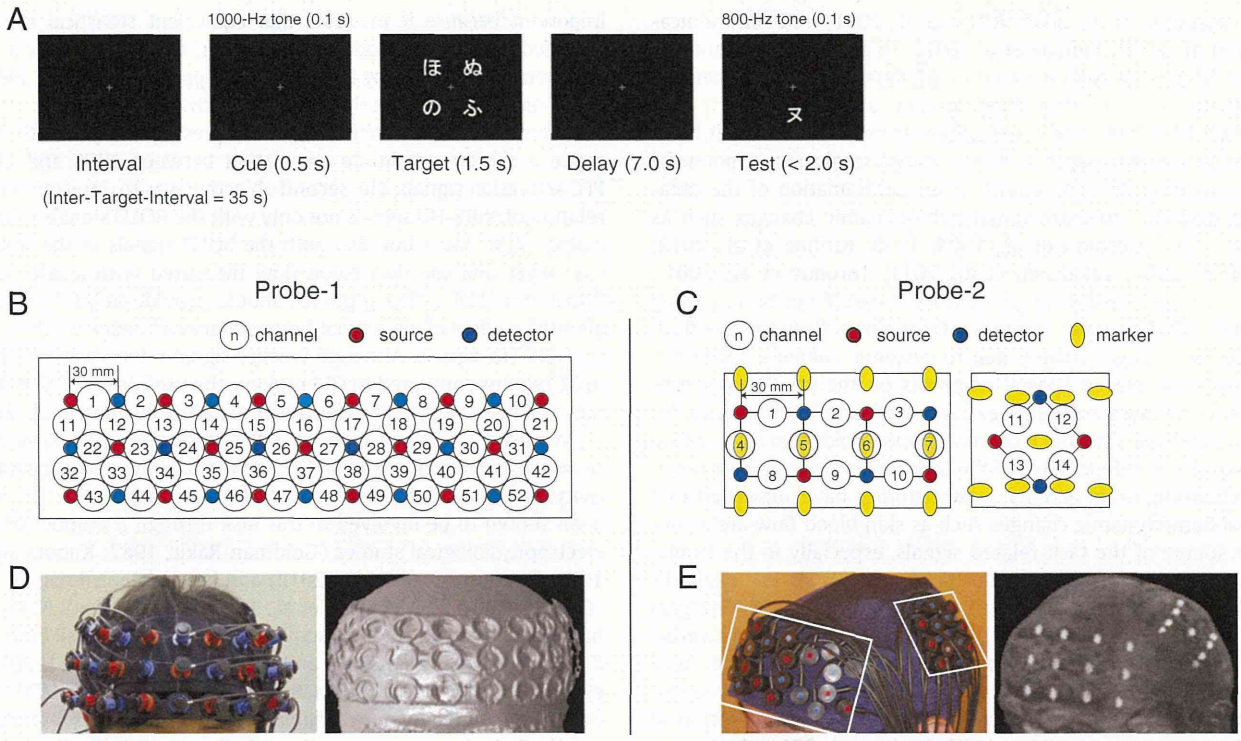

Fig. 1. Task paradigm and NIRS measurement setting. (A) Schematic diagram of WM task trial. (B) Configuration of measurement channels with unique numbers for Probe-1: there were 17 light-irradiating positions (red dots) and 16 detecting positions (blue dots). (C) Configuration of regular measurement channels (S–D distance of 30 mm) with unique numbers for Probe-2: there were six light-irradiating positions (red dots) and six detecting positions (blue dots). Positions of 21 vitamin E tablets used as markers are shown by yellow ellipses. Left part is placed on left prefrontal position; right part is placed on left parietal position. (D) Photograph of Probe-1 worn by representative participant (left) and corresponding T1-weighted image with probe holders, in which NIRS channel positions can be determined (right). (E) Photograph of Probe-2 worn by representative participant (left) and corresponding T1-weighted image with vitamin markers, in which the channel positions can be determined (right).

NIRS studies (Aoki et al., 2011, 2013; Sato et al., 2011a). Each task trial started with a 1500-ms presentation of the target stimuli for encoding (Target) on a PC display screen, which was followed by a delay of 7000 ms. A test stimulus for retrieval (Test) was then presented for 2000 ms or until the participant responded. The participant responded by pressing a button on a handheld box (Serial Response Box, Psychology Software Tools, Inc., U.S.A.) connected to the PC. The system recorded the button pressed and the reaction time. A Japanese *hiragana* character or a set of four such characters was presented as the Target, and a Japanese *katakana* character was presented as the Test. The participants were instructed to judge whether the Test character corresponded to the single Target character or to one of the four target characters and then press the appropriate button. They used the right index finger to press the "yes" button when the Test character corresponded to the Target character and used the right middle finger to press the "no" button when it did not correspond to the Target character. Because the characters presented as Target and Test were in different Japanese morphograms (i.e., *hiragana* and *katakana*), the participants made their judgments on the basis of the phonetic information conveyed by the characters, not on the basis of their form. In 12 task trials, the one-character Target (1-item) and four-character Target (4-item) conditions were randomized with the same probability. The probabilities of "yes" and "no" responses were controlled to be the same (50%). The interval between Target onset and the subsequent Target onset was set to 35 s. Only a fixation cross was presented during the interval and delay period. In addition, auditory cues (1000- and 800-Hz pure tones of 100-ms duration) were presented at the Target and Test onsets, respectively. The behavioral results for the WM task are shown in the Supplementary Materials (Table S1).

Finger tapping task

A simple finger-tapping task was used as a sensorimotor task. It was similar to that used in previous NIRS studies (Sato et al., 2005, 2006). The participants were instructed to watch a white fixation cross shown at the center of the screen. During the task period, the color of one half of the horizontal bar turned yellow at a rate of 3 Hz, and the participants were asked to tap their fingers in synchrony with the blinking timing of the horizontal bar in the fixation cross. During each task period, the fingers of one hand were repeatedly placed on the tip of the thumb in the following order: forefinger–second finger–third finger–little finger–third finger–second finger–forefinger. Each task period lasted for 15 s, and the interval between task periods was 25 s. The experiment consisted of ten task periods with the order of the right and left finger conditions alternating.

Data acquisition

NIRS

We used an optical topography system (ETG-4000, Hitachi Medical Corporation, Japan) for the NIRS measurements. The light sources consisted of continuous laser diodes with two wavelengths, 695 and 830 nm. The transmitted light (detected with avalanche photodiodes) was sampled every 100 ms. The optical fibers used for both the irradiating and detecting lights, including the points where the optical fibers were attached to the skin, are referred to as 'probes' ('source probes' and 'detecting probes').

We used two types of probe holders with different probe configurations (Figs. 1B–E). "Probe-1" was a conventional probe holder with 30-mm spacing between the source and detector (S–D) probes, covering a wide area mainly on the forehead. Seventeen light sources

and 16 detectors were arrayed in a 3 × 11 lattice pattern with 30-mm separation, forming 52 measurement positions (defined as 'channels'), one for each S–D pair (Fig. 1B). The probes were embedded in a soft silicon holder that was placed on the participant's forehead (Fig. 1D left). The probe holder is visible in a normal T1-weighted image (Fig. 1D right), so the spatial position of the probes could be registered in the MRI data. It was used for 15 participants (11 males and 4 females, mean age of 35.5, age range of 27–45).

"Probe-2" was a custom-made probe holder with both conventional S–D distance (30-mm) probes (Fig. 1C) and shorter S–D distance (15-mm) probes (not shown). The data collected with the shorter S–D distance probes were not used in the present study because it focuses on the quality of NIRS-Hb signals obtained with a conventional S–D distance of 30 mm. The shorter S–D distance results will be reported elsewhere. For the 30-mm measurements, 6 light sources and 6 detectors were arrayed in a lattice pattern, forming 14 measurement positions. Twenty-one vitamin E tablets were also attached to the probe holder as markers to identify the positions of the NIRS channels in the MRI images (Figs. 1C, E). This probe was used for the other 12 male participants (mean age of 37.7, age range of 30–48).

Data from both Probe-1 and the conventional S–D probes in Probe-2 were used for our main objective, i.e., determining the validity of activation signals in those areas commonly measured with both probe holders. In addition, we used all channel data from Probe-1 to examine the spatial characteristics of the correlation between the NIRS and BOLD signals. The experimental setup and task sequences were common to both probe holders.

Magnetic resonance imaging (MRI)

The MR imaging was performed with a Philips Achieva 3.0 T TX system (Philips Medical Systems, The Netherlands) with a 32-channel SENSE head coil. A total of 180 and 175 T2*-weighted gradient-echo echo-planar images (EPIs) were acquired while a participant underwent a single session of the TAP and WM tasks, respectively. A single EPI volume consisted of 35 3-mm-thick axial slices interspaced by a 1-mm gap, covering the entire brain. Other imaging parameters included TR = 2500 ms, TE = 30 ms, flip angle = 80°, field of view = 192 × 192 mm, and matrix = 64 × 64. Following the functional imaging, a B0 field map was acquired in the same head position (35 4-mm-thick axial slices, TR = 20 ms, TEs = 2.3/4.6 ms), which was later used to reduce image distortion caused by inhomogeneity in the magnetic field. Further, for anatomical identification of activated regions in the brain, a T1-weighted structural image was obtained (field of view = 250 × 250 mm, in-place resolution = 1.1 × 1.1 mm, 301 contiguous sagittal slices of 0.6 mm thickness, TR = 7.4 ms, TE = 3.4 ms, flip angle = 8°).

Laser-Doppler flowmetry

The skin blood flow was measured with a laser Doppler flowmeter (Microflow DSP, Oxford Optronix Ltd., UK) that had two surface probes. One was attached to the skin, centered between the eyebrows (channel 1), and the other was attached to the left temple (channel 2). The LDF analog output was converted into a digital signal with an analog-to-digital (A/D) converter (NR-2000, Keyence Corporation, Japan).

Data analysis

We primarily used MATLAB (The MathWorks, Inc., U.S.A.) for the analysis. A flow chart of the data analysis is shown in Fig. 2.

Registration of NIRS measurement area in structural MRI

To compare the temporal changes in the Hb signals from the NIRS measurements and in the BOLD signals from the fMRI measurements, we registered the NIRS channel positions in the structural MRI (Fig. 2A).

First, the T1-weighted image was coregistered to the mean functional image by using Statistical Parametric Mapping Software 8 (SPM8; Institute of Neurology, University College London, UK; run on MATLAB) (Step A-1). Then, the coordinates of the S–D pairs were obtained for each participant and each NIRS channel (NIRS-ch). This process (Step A-2) was done by manually identifying the positions of the sources and detectors in the probe holder shown in the T1-weighted image for Probe-1. For Probe-2, the position of each marker (a vitamin E tablet) was first manually identified in the T1-weighted image, and the coordinates of the sources and detectors were calculated from the marker positions. In parallel with these processes, the T1-weighted image was segmented using the "New Segment" routine in SPM8 into six components: gray matter, white matter, cerebrospinal fluid, soft tissue, bone, and air (Step A-3). Using the spatial information for the NIRS channels and the segmented MR images, we conducted two kinds of anatomical identifications of NIRS channels.

(1) Determination of BA numbers for NIRS channels
We determined the BA number for each NIRS channel to clarify the anatomical information. After we normalized the T1-weighted image with channel-position information into the Montreal Neurological Institute (MNI) space using SPM (Step A-4), we defined the measurement position for each NIRS channel as the midpoint between the source and detector. Next, we projected each measurement position onto a template of gray matter ("grey.nii" in spm8\tmp) and obtained the MNI coordinates for each participant (Step A-6). The projection point was defined as the voxel closest to the measurement position that showed an intensity greater than 0.5 in the template image. The 0.5 intensity threshold means that the voxel can be classified as being in the gray matter with a probability greater than 50% because the intensity of the template image for tissue ranges from 0 to 1 with the limitation that the sum of the intensities of all segmentation templates is 1. From the MNI coordinates, the BA number was determined (Rorden and Brett, 2000) for each projection point (Step A-8).

(2) Determination of spatial sphere for analysis (SFA)
We defined a spatial sphere of fMRI voxels for analysis (SFA), which corresponded to the measurement area for each NIRS channel. In step A-5, the photon-path-distribution function $P_n(x, y, z)$ at position r (x,y,z) was derived using the S–D coordinates and Eq. (1) (Feng et al., 1995; Sassaroli et al., 2006):

$$P_n(x,y,z) = \frac{z^2 \exp\left(-k\left[\left(x^2+y^2+z^2\right)^{1/2} + \left\{(d-x)^2+y^2+z^2\right\}^{1/2}\right]\right)}{\left(x^2+y^2+z^2\right)^{3/2}\left\{(d-x)^2+y^2+z^2\right\}^{3/2}} \times \left\{k\left(x^2+y^2+z^2\right)^{1/2}+1\right\}\left[k\left\{(d-x)^2+y^2+z^2\right\}^{1/2}+1\right] \quad (1)$$

Function P_n (x, y, z) represents the proportional probability of the photon path distribution, where a photon irradiated at (0, 0, 0) and detected at (d, 0, 0) crosses the generic point (x, y, z). The effective attenuation coefficient k is defined as $\sqrt{3\mu_a\mu_s'}$, where absorption coefficient μ_a is 0.011 mm^{-1} and the reduced scattering coefficient of tissue μ_s' is 1.2 mm^{-1} (Sassaroli et al., 2006). We set a threshold of P_n $(x, y, z) > 10^{-10}$ for the SFA (Step A-7 and Fig. 3A). We used the segmented MR images to identify the gray matter (GM) and soft tissue (ST) voxels in the SFA (Step A-9) for the subsequent analysis of both the cortical BOLD and extracranial BOLD signals. We focused on the GM region, which shows the cortical responses to experimental tasks, and on the ST region, which is presumed to show the skin blood flow changes (Fig. 3B).

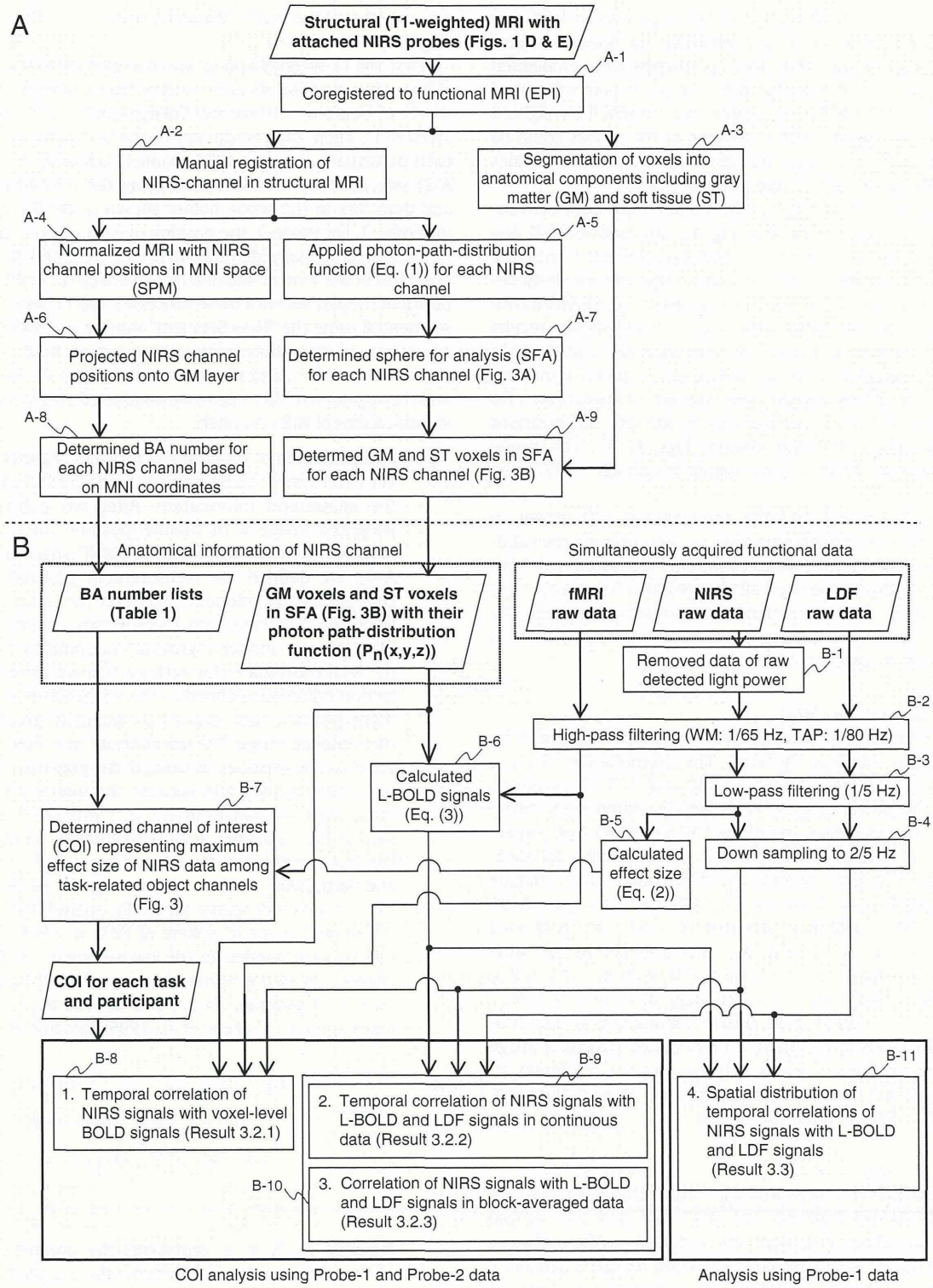

Fig. 2. Flowchart of basic analysis. Parallelograms represent input/output data, and rectangles represent processes. Each process is numbered as a step (A-1 to A-9 and B-1 to B-11) corresponding to explanation in text.

Functional signal preprocessing

The preprocessing of the simultaneously acquired fMRI, NIRS and LDF raw data are diagrammed in the lower right part of Fig. 2B.

NIRS. A portion of the NIRS signal preprocessing was performed using the plug-in-based analysis software Platform for Optical Topography Analysis Tools (developed by Hitachi, CRL; run on MATLAB). Prior to analysis, the data for channels with low detected light power were removed (Step B-1). The threshold for removal was set to a total gain of over 6667, which corresponds to the transmitted light being less than $10^{-9}\times$ the irradiation power. The main reason for the low detected light was probably poor probe attachment due to hair.

For each NIRS channel, the optical data for two wavelengths were transformed into a time series of Hb signals (oxy-Hb and deoxy-Hb

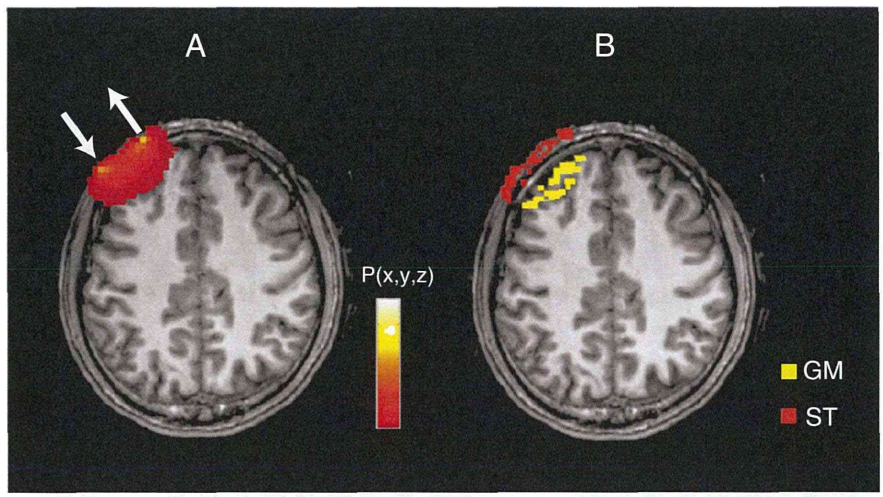

Fig. 3. Example images of spatial sphere for analysis in NIRS-channel 28 of Probe-1. (A) Proportional probability of photon path distribution as determined by simulation using photon-path-distribution function. (B) Voxels in gray matter (yellow) and those in soft tissue (red) in sphere as determined by data segmentation.

signals) on the basis of the modified Beer-Lambert law (Delpy et al., 1988; Maki et al., 1995). These signals were expressed as the product of the changes in hemoglobin concentration (mM) and optical path length (mm) in the activation region (effective optical path length). A high-pass filter was applied to the NIRS-Hb signals to remove low-frequency drift, which was longer than the twofold duration of one task sequence (WM: 1/65 Hz, TAP: 1/80 Hz) (Step B-2), and a low-pass filter was applied to the NIRS-Hb signals to remove components with a frequency higher than the sampling period in the fMRI scanning (2500 ms) (Step B-3). Finally, the filtered NIRS-Hb signals were down-sampled to the fMRI scanning frequency for comparison with the fMRI data (Step B-4).

After the filtering process, the effect size of the task-related signal change was calculated for each participant and each task (Eq. (2) and Step B-5) to determine the channel of interest. The effect size (Cohen's d) is similar to the contrast-to-noise ratio (CNR) used by Cui et al. (2011), which is the amplitude difference between the mean of the activation period ($mean(Act)$) and that of the control period ($mean(Con)$) divided by the pooled standard deviation (SD, σ) (Cohen, 1992):

$$d = \frac{mean(Act) - mean(Con)}{\sigma}$$
$$\sigma = \sqrt{\frac{\sum_{i}^{n_1}(y_{1i}-\bar{y}_1)^2 + \sum_{i}^{n_2}(y_{2i}-\bar{y}_2)^2\sqrt{2}}{n_1+n_2-2}}, \quad (2)$$

where y_1 and y_2 are the vectors of the raw NIRS-Hb signals in the activation and control periods, respectively. The activation period was commonly set to the interval from 5 s after onset to the task end (WM: 3.5 s, TAP: 10 s). The control period was set to the same duration (WM: 3.5 s, TAP: 10 s) before task onset.

fMRI. MR data preprocessing was performed using statistical parametric mapping software 8 (SPM8; Institute of Neurology, University College London, UK; run on MATLAB). First, raw functional images were unwarped by using the field map acquired for the participant and were spatially realigned to the mean image calculated from the entire data. We then applied to the BOLD time series the same band-pass filter used in the NIRS-Hb signal preprocessing (Step B-2). Unlike the standard preprocessing procedure, functional images were not normalized into the standard space but were instead analyzed in the participant's native space.

Using the anatomical information of NIRS channels obtained in step A-9, we calculated the photon-path-distribution average BOLD signal for each NIRS channel (Eq. (3)) as the layer BOLD (L-BOLD) signal for the GM and ST layers using a modified version of (Sassaroli et al., 2006)

$$\mathrm{L-BOLD(t)} = \frac{\int_V \mathrm{BOLD}_{raw}(x,y,z,t)P_n(x,y,z)dxdydz}{\int_V P_n(x,y,z)dxdydz}, \quad (3)$$

where L-BOLD(t) is the layer BOLD signal averaged using a weight given by the photon-path-distribution function, and BOLD_{raw} (x,y,z,t) is the raw BOLD signal for each voxel at time t and position (x,y,z) (Step B-6).

LDF. The same preprocessing as for the NIRS-Hb signals was used for the LDF signals. That is, the LDF signals were filtered using the same parameters and down-sampled to match the fMRI scanning frequency (Steps B-2, B-3 and B-4).

Selection of channel of interest (COI)

First, we defined the NIRS channels in BA 46 as the object channels for the WM task and those in BAs 1, 2, 3, 4, 5, 6, and 40 as the object channels for the TAP task (Fig. 4A). Next, we selected as the channel of interest (COI) for each task condition the object channel with the maximum effect size (mean effect size of oxy-Hb signal and deoxy-Hb signal) on the condition that the effect size exceeded 0.2 (Step B-7) (Fig. 4B). The 0.2 threshold corresponds to the "small" effect size (Cohen, 1992). Signal responses to the 4-item condition were used in the WM task, and those to the contralateral-hand tapping task were used in the TAP task. We focus on the COI for detailed analysis because our interest here is to investigate task-related NIRS-Hb signals. If we did not focus on the COI, the correlation with BOLD signals could be contaminated by the effects of noisy or non-activated channels.

Correlation analysis in COI

Using the fMRI signals in the SFA, we conducted three types of correlation analyses for COI using the data for both Probe-1 and -2.

(1) Correlation with voxel-level BOLD signals
Pearson's correlation coefficient (r) between the NIRS-Hb signal and the BOLD signal was calculated for each voxel in the GM and ST layers of the SFA (Step B-8). The significance of the correlation coefficient was determined using a false

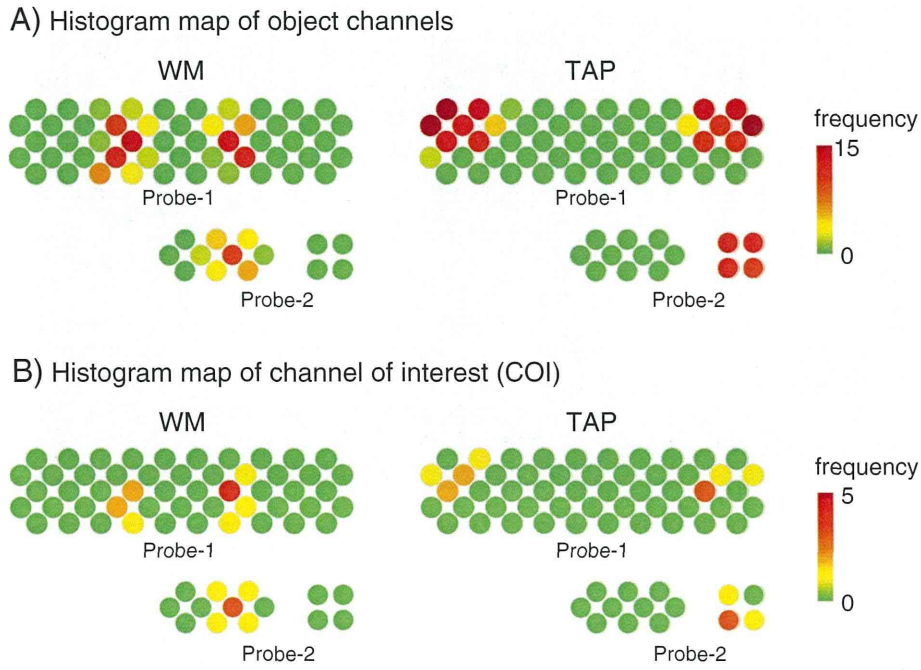

Fig. 4. Histogram maps of (A) object channels and (B) channel of interest. In (A), number of participants whose registration was in a target BA (BA 46 for WM task; BAs 1, 2, 3, 4, 5, 6, and 40 for TAP task) is indicated by frequency represented by color scale for each NIRS channel. In (B), number of participants in selected channel is indicated by color scale for each channel. Arrangement of NIRS channels on head is shown in Fig. 1.

discovery rate (FDR) control procedure (Genovese et al., 2002) (FDR corrected $p < 0.05$). The total numbers of voxels and correlated voxels were determined for both the GM and ST regions. A two-way analysis of variance (ANOVA) (layer × task) was used to examine the difference by layer type (GM or ST) and by task type (WM or TAP) for oxy- and deoxy-Hb signals.

(2) Correlation with L-BOLD signals
The continuous L-BOLD signals in the GM and ST layers (L-BOLD (GM) and L-BOLD (ST) signals) were used to calculate the correlation coefficients for the NIRS-Hb signals for each task (Step B-9). In addition, an LDF signal was used to calculate the correlation coefficients for the NIRS-Hb signals. For statistical examination, correlation coefficient r was converted into a Z-value using Fisher's Z-transformation (Eq. (4))(Fisher, 1915, 1921):

$$Z = \frac{1}{2}\ln\frac{1+r}{1-r}. \quad (4)$$

The correlation Z-values were tested using a one-sample t test against zero. The significance of the t-values under all conditions was determined by using a threshold corrected for multiple comparisons using the Bonferroni procedure (Bonferroni corrected $p < 0.05$, two-tailed).

(3) Correlation analysis for block-averaged activation signals
To examine the correlation of the task-related responses in more detail, we calculated time-locked block-averaged timecourses for the NIRS, L-BOLD, and LDF signals for each task condition and each participant (Step B-10). First, the time-continuous data were separated into task blocks: a WM task block was defined as 14 scans (35-s) period starting 2 scans (5-s) before the Target onset and ending 12 scans (30-s) after the onset, and a TAP task block was defined as 17 scans (42.5-s) period starting 3 scans (7.5-s) before the task onset and ending 14 scans (35-s) after the onset. Each task block was shifted to make the average value during the pre-task period (including the task onset) zero as the baseline. Then, the task blocks were averaged for each task and each participant and used as the block-averaged signals. Using the block-averaged signals, we calculated the task-related response amplitudes as the average value during the activation periods. The activation period for the WM task was defined as three scans (7.5 s) from the second scan after Target onset, and that for the TAP task was defined as five scans (12.5 s) from the third scan after task onset. To examine the linearity of the response amplitudes between the NIRS and L-BOLD signals, we calculated the correlation coefficients across participants. We additionally calculated effect sizes using Eq. (2) and data from before the averaging process to examine the signal-to-noise ratio (SNR) for the task-related response for each signal.

Correlation analysis for multiple NIRS channels

The correlation coefficients between the continuous NIRS and L-BOLD (GM) signals were calculated for all NIRS channels in the Probe-1 data to examine the generality and spatial variability of the correlation between the NIRS and fMRI signals (Step B-11). On the basis of the correlation coefficients under four conditions (oxy-Hb in WM, deoxy-Hb in WM, oxy-Hb in TAP, deoxy-Hb in TAP), the 52 NIRS channels were clustered into three areas using K-means clustering in MATLAB (MathWorks, Inc., U.S.A.) to determine the area dependency of the correlation coefficients.

Results

Selection of COI

The BA number was determined for each NIRS channel for each participant in accordance with the registration of NIRS channels in the MNI space (Table 1). Frequency maps of the object NIRS channels (BA 46 for WM task; BAs 1, 2, 3, 4, 5, 6, and 40 for TAP task) showed that both probe holders covered the regions of interest, i.e., the dorsolateral PFC and the sensorimotor cortex (Fig. 4A). A COI was not

Table 1
Estimated location of each NIRS channel in Probe-1 and Probe-2 on normalized brain image. Mean and standard deviation (SD) of MNI coordinates across participants and corresponding Brodmann area (BA) numbers are shown for each channel. Percentage of participants by BA number is shown in parentheses.

Ch	Mean MNI coordinates			SD			
	x	y	z				
Probe-1							
1	58.8	−22.5	51.3	5.1	3 (40%)	1 (40%)	2, 4, 6 (7%)
2	54.3	0.4	49.5	6.5	6 (80%)	4 (13%)	44 (7%)
3	44.8	23.2	47.9	6.2	9 (73%)	45 (13%)	6, 46 (7%)
4	30.0	40.0	46.7	6.3	9 (67%)	8 (20%)	46 (13%)
5	10.3	50.1	46.8	7.3	9 (80%)	8 (13%)	10 (7%)
6	−8.9	50.0	46.7	6.9	9 (87%)	8 (7%)	10 (7%)
7	−29.1	38.3	46.4	5.2	9 (80%)	46 (13%)	8 (7%)
8	−44.1	20.9	47.5	5.7	9 (87%)	45 (13%)	-
9	−53.3	−0.4	48.0	7.0	6 (93%)	44 (7%)	-
10	−58.5	−25.5	48.9	5.4	3 (40%)	2, 40 (20%)	1 (13%)
11	64.1	−34.3	43.5	3.9	40 (73%)	2 (20%)	1 (7%)
12	62.8	−7.7	39.2	5.3	3 (40%)	1 (27%)	6 (20%)
13	55.5	17.1	36.8	4.8	44 (47%)	6 (33%)	45 (13%)
14	43.7	38.7	35.1	5.7	46 (67%)	45 (20%)	9 (13%)
15	23.1	54.9	35.3	6.3	9 (73%)	46 (20%)	10 (7%)
16	1.6	59.2	36.4	4.6	9 (73%)	10 (27%)	-
17	−22.5	53.9	35.3	5.9	9 (67%)	46 (27%)	10 (7%)
18	−42.4	37.5	34.1	5.5	45 (47%)	46 (40%)	9 (13%)
19	−53.7	15.2	36.3	5.5	44 (53%)	9 (27%)	45 (13%)
20	−62.0	−10.5	37.6	5.2	1 (47%)	43 (27%)	3 (13%)
21	−62.9	−36.0	41.9	4.0	40 (87%)	2 (13%)	-
22	67.7	−19.3	30.5	3.3	2 (73%)	43 (13%)	1 (13%)
23	63.1	7.9	26.5	4.1	6 (73%)	4, 43, 44, 45 (7%)	
24	53.3	33.3	24.0	5.9	45 (80%)	44 (13%)	46 (7%)
25	36.8	54.3	23.9	4.6	46 (93%)	10 (7%)	-
26	12.5	65.3	24.0	5.1	10 (93%)	9 (7%)	-
27	−12.1	64.4	24.7	5.3	10 (87%)	9 (13%)	-
28	−36.4	52.5	23.1	5.6	46 (87%)	10 (13%)	-
29	−51.6	32.4	22.5	5.4	45 (100%)	-	-
30	−61.2	6.4	24.7	5.5	6 (73%)	43 (20%)	44 (7%)
31	−66.0	−21.2	29.2	4.7	2 (67%)	43 (27%)	40 (7%)
32	69.6	−32.0	13.6	3.4	22 (87%)	2, 40 (7%)	-
33	67.2	−4.3	13.6	3.5	22 (40%)	43 (33%)	48 (27%)
34	58.8	26.3	11.9	3.6	45 (67%)	44 (33%)	-
35	46.9	49.7	10.1	4.8	46 (80%)	45 (13%)	10 (7%)
36	25.6	65.5	11.2	4.9	10 (67%)	11 (20%)	46 (13%)
37	−0.5	68.8	11.6	4.3	10 (93%)	11 (7%)	-
38	−25.7	64.1	11.6	4.9	10 (87%)	11, 46 (7%)	-
39	−45.7	48.4	9.2	4.5	46 (80%)	45 (20%)	-
40	−57.2	25.1	10.8	5.8	45 (67%)	44 (27%)	47 (7%)
41	−65.1	−6.5	11.9	4.5	43 (40%)	22 (33%)	21 (7%)
42	−67.6	−34.7	13.3	5.0	22 (80%)	21 (13%)	48 (7%)
43	69.7	−16.9	−4.0	2.2	21 (60%)	22 (40%)	-
44	60.7	10.5	−3.1	4.6	38 (40%)	48 (40%)	21 (20%)
45	52.9	41.2	−3.5	3.8	46 (47%)	45 (40%)	47 (13%)
46	38.3	60.3	−1.3	3.4	10 (60%)	46, 47 (20%)	-
47	14.9	69.3	−0.7	3.7	11 (53%)	10 (47%)	-
48	−13.7	69.1	0.0	4.3	10 (53%)	11 (47%)	-
49	−37.7	59.3	−1.7	3.8	10 (73%)	47 (20%)	46 (7%)
50	−52.0	38.9	−3.9	3.6	45 (73%)	47 (27%)	-
51	−59.6	8.0	−3.5	5.3	48 (40%)	38 (33%)	21 (20%)
52	−67.7	−18.8	−5.1	4.5	21 (67%)	22 (33%)	-
Probe-2							
1	−5.8	57.8	38.5	4.2	9 (83%)	10 (17%)	-
2	−24.7	50.7	37.7	4.7	9 (58%)	46 (42%)	-
3	−42.5	36.8	34.7	4.2	45 (42%)	46 (33%)	9 (25%)
4	5.5	65.2	25.7	4.8	10 (92%)	9 (8%)	-
5	−15.0	62.2	27.2	4.9	10 (67%)	9 (17%)	46 (17%)
6	−36.2	50.7	26.2	4.5	46 (83%)	45 (17%)	-
7	−50.7	34.3	21.8	4.4	45 (83%)	46 (8%)	44 (8%)
8	−7.2	68.7	14.5	4.8	10 (100%)	-	-
9	−27.3	62.5	15.0	4.0	10 (75%)	46 (25%)	-
10	−44.5	48.8	12.2	3.9	46 (50%)	45 (42%)	10 (8%)
11	−52.0	−23.3	57.0	5.5	3 (33%)	4 (33%)	1, 40 (17%)
12	−48.0	−37.8	59.2	3.9	40 (58%)	3 (33%)	1 (8%)
13	−61.5	−29.0	44.7	4.7	40 (42%)	2, 3 (25%)	1 (8%)
14	−56.5	−46.5	48.0	4.0	40 (83%)	39 (17%)	-

selected for 8 participants in the WM task and 11 participants in the TAP task because there were no channels meeting the two criteria described above. Failure to meet the first criteria resulted from a failure to detect enough light power in the TAP task (eight participants showed no object channels with sufficient light power), possibly because the sensorimotor area corresponded to haired regions. Failure to meet the threshold of effect size resulted from a failure to detect a reliable response to the task. This resulted in the removal of eight participants from the WM task data and three participants from the TAP task data. We thus analyzed the COI signals for 19 and 16 participants for the WM and TAP tasks, respectively (Fig. 4B). The results of correlation analysis using the COI data are presented in the following sub-sections.

Correlation of NIRS-Hb signals with BOLD and LDF signals for COI

Temporal correlation of NIRS-Hb signals with voxel-level BOLD signals

First, to investigate the general tendency, we compared the continuous data, i.e., the data for the entire duration of the experiment, between the NIRS and BOLD signals. Representative results for two participants are shown in Fig. 5. Voxel-level correlation analysis revealed that the majority of GM voxels in the SFA had significant correlation coefficients for both the WM (Fig. 5A) and TAP (Fig. 5C) tasks whereas only a few ST voxels had significant coefficients. Moreover, the L-BOLD (GM) signals were highly correlated with both the oxy-Hb and deoxy-Hb signals within participant (Figs. 5B and D).

The mean data values for the voxel-level analysis for the participants with a COI are shown in Table 2. A two-way ANOVA (layer type×task type) for the total number of voxels showed a significant interaction between layer type and task type ($F\ (1, 66) = 11.4$, $p < 0.005$) without any main effects (layer type: $F\ (1, 66) = 3.4$, $p = 0.07$; task type: $F\ (1, 66) = 2.3$, $p = 0.13$). This means that the total number of voxels was larger for ST than for GM in the sensorimotor area (TAP task) and that the opposite case held for the PFC (WM task). Nonetheless, the number of correlated voxels for GM (mean = 118–162) was clearly larger than that for ST (mean 7–17) for both tasks (Table 2). The two-way ANOVA (layer type×task type) for the number of correlated voxels revealed a clear significance for the main effects of layer signal ($F\ (1, 66) = 59.1$ for oxy-Hb and $F\ (1, 66) = 37.0$ for deoxy-Hb, $p < 0.00001$) without the main effects of task type ($F\ (1, 66) = 1.5$, $p = 0.22$ for oxy-Hb and $F\ (1, 66) = 0.2$, $p = 0.67$ for deoxy-Hb) or interaction ($F\ (1, 66) = 2.3$, $p = 0.14$ for oxy-Hb and $F\ (1, 66) = 0.0$, $p = 0.94$ for deoxy-Hb).

Temporal correlation of NIRS-Hb signals with L-BOLD and LDF signals in continuous data

The correlation coefficients of the NIRS-Hb signals for the L-BOLD (GM), L-BOLD (ST), and LDF signals were statistically examined across participants (Fig. 6). First, the *Z*-values for each condition were tested by performing a one-sample *t*-test against zero across participants in which the *p*-value was corrected for the multiple (12×) comparisons. On the one hand, the L-BOLD (GM) signals showed significant correlation coefficients with the oxy-Hb signals (WM: $t(18) = 8.2$, $p < 5 \times 10^{-6}$; TAP: $t(15) = 4.8$, $p < 5 \times 10^{-3}$) and with the deoxy-Hb signals (WM: $t(18) = 4.4$, $p < 5 \times 10^{-3}$; TAP: $t(15) = 5.2$, $p < 5 \times 10^{-3}$) (Fig. 6A). The two-way ANOVA (task type × Hb type) showed a generality of the NIRS–BOLD relationship as no main effect of task type ($p = 0.37$) and Hb type ($p = 0.24$) with no interaction ($p = 0.73$) were indicated. On the other hand, the L-BOLD (ST) signals showed no significant correlation coefficients with any of the NIRS-Hb signals ($p > 0.2$) (Fig. 6B).

Because use of the extracranial BOLD signal has not become standard, the same correlation analysis was conducted using LDF signals instead of L-BOLD signals (Fig. 6C). As the temporal LDF signals in the two channels were significantly correlated within participants in most cases (mean ± SD of $r = 0.52 \pm 0.22$, $p < 0.0001$ for 25 of 27 participants), only the LDF signal in channel 1 (centered between